Bénard convection from a circular cylinder in a packed bed ☆

Gazy F. Al-Sumaily [a,b,*], Mark C. Thompson [b]

[a] Fluids Laboratory for Aeronautical and Industrial Research (FLAIR), Department of Mechanical and Aerospace Engineering, Monash University, Victoria 3800, Australia
[b] Department of Mechanics and Equipments Engineering, University of Technology, Baghdad, Iraq

ARTICLE INFO

ABSTRACT

Bénard convection around a circular heated cylinder embedded in a packed bed of spheres is studied numerically. The *Forchheimer–Brinkman–extended* Darcy momentum model with the *Local Thermal Non-Equilibrium* energy model is used in the mathematical formulation for the porous layer. The governing parameters considered are the Rayleigh number ($10^3 \leq Ra \leq 5 \times 10^7$) and the thermal conductivity ratio ($0.1 \leq k_r \leq 10{,}000$). The structural properties of the packed bed are kept constant as: cylinder-to-particle diameter ratio $D/d = 20$ and porosity $\varepsilon = 0.5$, while the Prandtl number is fixed at $Pr = 0.71$. It is found that the presence of the porous medium suppresses significantly the strong free convection produced in the empty enclosure, and reduces considerably the high intensity of the pair of vortices generated behind the cylinder. Also, the results show that the porous medium can play the role of insulator or enhancer of heat transfer from the heat source, depending mainly on their thermal conductivities regardless of the Rayleigh number.

© 2014 Elsevier Ltd. All rights reserved.

1. Introduction

Buoyancy-induced flow over horizontal heated cylinders in porous media is relevant to several engineering problems especially those involve thermal insulators. The thermal insulator typically includes a fibrous porous material, which is permeable to fluid motion. Consequently, natural convection may develop in the insulating material and contribute significantly to the heat transfer process, as has been demonstrated by many authors. Eckert and Drake [5] and Thiyagarajan and Yovanovich [21] represent early studies in this regard, but they have concentrated on the case of immersed cylinders assuming the surrounding porous medium to be solely conductive. However, for a high-permeability porous medium, the assumption of pure conduction heat transfer from an immersed cylinder may not be valid. In fact, the medium which is permeable enough to fluid motion produces a temperature difference between the heated cylinder and the fluid penetrating within the medium, giving rise to a natural convection flow. Therefore, the entire heat transfer from buried cylinders consists of both convection as well as conduction, and in the many cases the contribution of free convection is as large or larger than that of conduction.

The first similarity solutions for free convection adjacent to axisymmetric and two-dimensional bodies of arbitrary shaped cylinders and spheres, in a constant porosity medium of infinite extent were obtained by Merkin [16] based on the Darcy's law in the boundary layer. Using the same approach, Cheng [3] proposed a theoretical correlation for the average Nusselt number, to the specific case of a horizontal circular cylinder heated at constant temperature. Fand et al. [7] performed the first experimental investigation on free convection heat transfer from a cylinder buried in a randomly packed bed of glass spheres saturated by either water or silicone oil. They concluded that the whole range of Rayleigh number (Ra) can be divided into two low and high regions. In each region, the behaviour of the Nusselt number is totally different. The results showed that the high-Ra region, which is usually located near the heated surface, corresponds to the *Forchheimer* flow, whereas, the low-Ra region, somewhat further from the surface, corresponds to the *Darcy* flow.

Ingham and Pop [12] investigated numerically the problem under the assumption of the flow being governed by Darcy's law for the full range of Rayleigh number. They found it difficult to obtain accurate numerical solutions at small values of Ra, while the asymptotic solutions are only valid for $-\log(Ra) \gg 1$. For $Ra \approx 1.0$, the numerical results were found to be in a reasonable agreement with the experimental findings of Fand et al. [7]. However, at larger Ra, there was a need for numerical solutions to the boundary-layer equations, but with an increasing difference between them and the experimental data as Ra increases. However, this difference should not be surprising because at large Ra the experimental results correspond to the *Forchheimer* model, thus the application of Darcy's law loses validity. Later, numerical and experimental investigations of free convection around a cylinder heated with constant heat flux were performed by Himasekhar and Bau [10]. The results of the measured average Nusselt number were found to be higher

---

<table>
</table>

Nomenclature

a_{sf}	specific interfacial area, (m^{-1}).
Bi	Biot number, $Bi = D^2 h_{sf} a_{sf}/k_s$.
C_F	inertial coefficient, $C_F = 1.75/\sqrt{150\varepsilon^3}$.
d	particle diameter, (m).
D	cylinder diameter, (m).
Da	Darcy number, $Da = K/D^2$.
h_{sf}	interfacial heat transfer coefficient, $(W/m^2 \cdot K)$.
H	packed bed height, (m).
k_f	fluid thermal conductivity, $(W/m \cdot K)$.
k_s	solid thermal conductivity, $(W/m \cdot K)$.
$k_s t$	stagnant thermal conductivity, $(W/m \cdot K)$.
k_r	solid/fluid thermal conductivity ratio, $k_r = k_s/k_f$.
K	permeability of the porous medium, $K = \varepsilon^3 d^2/150(1-\varepsilon)^2 (m^2)$.
L	packed bed length, (m).
Nu	Nusselt number.
p_f	fluid pressure, (N/m^2).
P_f	dimensionless fluid pressure, $P_f = p_f D^2/\rho_f \alpha_f^2$.
Pr	Prandtl number, $Pr = \nu_f/\alpha_f$.
Ra	Rayleigh number, $Ra = g\beta D^3(T_h - T_c)/\alpha_f \nu_f$.
Re_p	particle Reynolds number, $Re_p = \rho_f |u| d/\mu_f$.
S	circumference of the cylinder, (m).
T	temperature, (K).
u	horizontal velocity component, (m/s).
U	dimensionless horizontal velocity component, $u = uD/\alpha_f$.
v	vertical velocity component, (m/s).
V	dimensionless vertical velocity component, $V = vD/\alpha_f$.
x, y	horizontal and vertical coordinates, (m).
X, Y	dimensionless horizontal and vertical coordinates, $X = x/D, Y = y/D$.

Greek symbols

ε	porosity.
θ	dimensionless temperature, $\theta = (T - T_c)/(T_h - T_c)$.
μ_f	fluid dynamic viscosity, $(kg/m \cdot s)$.
ρ_f	fluid density, (kg/m^3).
ν_f	fluid kinematic viscosity, (m^2/s).
φ	angular coordinate, (o).

Subscripts

eff	effective.
f	fluid.
s	solid.
t	total.

than those obtained from the numerical solutions at large Rayleigh number. The numerical solutions were obtained using the Darcy's approximation with the assumption of negligible thermal dispersion. They attributed the difference between their theoretical and experimental results at high Ra to the flow transition from a steady two-dimensional flow to a transient three-dimensional one as observed in their experiments.

Oosthuizen and Naylor [17] examined free convection heat transfer from a cylinder placed in a square enclosure partly filled with a layer of air-saturated porous medium and partly filled with a layer of only air, with a horizontal impermeable barrier between the two layers. The cylinder was buried in the porous layer, and the barrier was assumed to offer a negligible resistance to heat transfer. The main objective of the study was to determine how the rates of heat transfer from the cylinder are influenced by the size of the air-gap at the top of the enclosure for the different Rayleigh numbers, solid-to-fluid thermal conductivity ratios,

Darcy numbers and enclosure sizes. In all cases considered, a certain critical size of the fluid layer thickness was found to give a minimum Nusselt number. Saada et al. [19] analysed the flow and heat transfer characteristics of natural convection about a cylinder coated by an air-saturated fibrous layer by using a mathematical model incorporating non-Darcian effects. They did an optimisation study in order to find the best combination of parameters: coating layer thickness, effective/stagnant thermal conductivity ratio and Darcy number Da, that produce good thermal insulation or heat transfer augmentation. The results demonstrated that the efficient insulation, which corresponds to heat losses less than 10 %, can be obtained for layer thicknesses higher than 0.8 cylinder diameters, for low $Da \leq 10^{-7}$ and conductivity ratio equal to 2. Whereas, for heat transfer enhancement purposes, the study found that a highly permeable and highly conducting porous layer is suitable. Unsteady free convective flow over a cylinder buried in a semi-infinite porous medium bounded above by a liquid layer was studied by Kumari and Nath [15]. It was assumed that the flow is described by Darcy's law due to the small range of Rayleigh numbers ($Ra < 200$) used. The unsteadiness condition in the problem arose from the cylinder, which is suddenly isothermally heated or cooled and then maintained at that temperature. The average Nusselt number was shown to be significantly influenced by Ra and the ratio of burial depth to cylinder diameter. The Nusselt number increases as Ra increases at a constant value of burial depth ratio; however, it can be increased or decreased as the burial depth ratio increases depending on Ra.

To the authors' knowledge, the literature reveals that the problem of free convection about a cylinder embedded in an enclosed packed bed of spherical particles has been previously investigated only by Fand et al. [7] experimentally, as mentioned above, and studied numerically only by Hsiao et al. [11]. In this study, both uniform wall temperature and uniform heat flux thermal boundary conditions were considered at the cylinder surface. In addition, both non-Darcian effects and thermal dispersion effects were taken into account. The results illustrated that these effects have an appreciable influence on the heat transfer enhancement from the cylinder's surface. Also, it was deduced that with these effects considered simultaneously, the predicted Nusselt number was in better agreement with the experimental results of Fand et al. [7] and Himasekhar and Bau [10]. However, thermal equilibrium was assumed in the packed bed. The thermally non-equilibrium energy model was used, with the Darcy's approximation, by Saeid [20] to numerically study natural convection in the boundary layer around an isothermal horizontal cylinder immersed in a fibrous porous medium. The effect of the interfacial heat transfer coefficient parameter and the porosity-scaled thermal conductivity ratio parameter on the local and average Nusselt numbers was investigated. The results showed that an increase in either of these two parameters results in an increase in the total average Nusselt number throughout the fluid and solid phases. However, it was found that the dependency of the total Nusselt number on the related parameters is different. This depended substantially on the conductivity ratio parameter and only slightly on the interfacial heat transfer parameter.

The aim of this work is to examine numerically the Bénard convection from a circular horizontal cylinder embedded in a packed bed of spheres using a non-Darcy model with *Local Thermal Non-Equilibrium* (*LTNE*). Our study extends the previously published articles. Reviewing the literature, all the published articles have used the thermal equilibrium assumption. Therefore, this extension to *LTNE* can be considered as a new contribution of this article. The effect of the existence of the porous medium for different materials and at different Rayleigh numbers, on the flow development, temperature distribution, and the heat transfer rate, will be presented in some detail.

2. Problem description

Fig. 1 describes the physical problem under consideration along with the chosen coordinate system. As shown, a horizontal circular cylinder
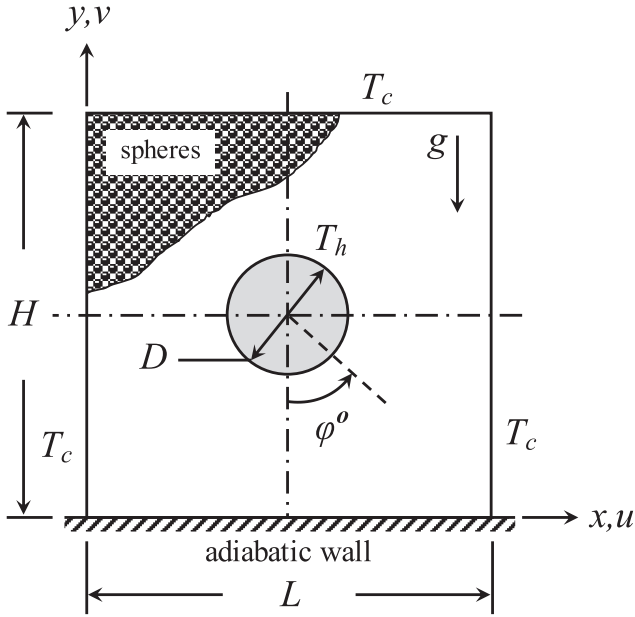
Fig. 1. Physical model and coordinate system.

of diameter D and surface temperature T_h is buried in a two-dimensional enclosed packed bed of spheres of overall height $H = 4D$ and length $L = 4D$. The bed is bounded on all four sides by impermeable boundaries. The lower horizontal wall is adiabatic, while other walls are held at a constant temperature T_c. It is assumed that at time $t > 0$, the cylinder surface is suddenly heated to T_h, and subsequently maintained at that temperature. This sudden change in the temperature introduces potential unsteadiness in the system, i.e., $T_h > T_c$, causing a buoyancy driven laminar flow.

3. Basic equations

We assume that the convective, incompressible, viscous fluid flow is described by the *Brinkman–Forchheimer–extended Darcy* (generalized model) model and that the Boussinesq approximation is valid. It is also assumed that the gravity acts in a downward vertical direction and that the fluid properties are constant except for the density. In addition, the following assumptions are also applied: the porous medium is homogenous and isotropic; no heat generation occurs inside the porous medium; the inter-particle radiation heat transfer is ignored; and the medium is saturated with fluid. Importantly, the medium and fluid can be in *Local Thermal non-Equilibrium* everywhere. Under these assumptions, the continuity, momentum and energy equations can be written in a dimensionless form as follows:

$$\frac{\partial U}{\partial X} + \frac{\partial V}{\partial Y} = 0, \tag{1}$$

$$\frac{1}{\varepsilon^2}\left(U\frac{\partial U}{\partial X} + V\frac{\partial U}{\partial Y}\right) = -\frac{Pr}{Da}U - \frac{C_F}{\sqrt{Da}}|\vec{U}|U + \frac{Pr}{\varepsilon}\left(\nabla^2 U\right) - \frac{\partial P_f}{\partial X}, \tag{2}$$

$$\frac{1}{\varepsilon^2}\left(U\frac{\partial V}{\partial X} + V\frac{\partial V}{\partial Y}\right) = -\frac{Pr}{Da}V - \frac{C_F}{\sqrt{Da}}|\vec{U}|V + \frac{Pr}{\varepsilon}\left(\nabla^2 V\right) - \frac{\partial P_f}{\partial Y} + RaPr\theta_f, \tag{3}$$

$$\varepsilon\left(U\frac{\partial \theta_f}{\partial X} + V\frac{\partial \theta_f}{\partial Y}\right) = \nabla\cdot\left(\frac{k_{f.eff,(x,y)}}{k_f}\nabla\theta_f\right) + Bi\ k_r\left(\theta_s - \theta_f\right), \tag{4}$$

$$(1-\varepsilon)\left(\nabla^2\theta_s\right) - Bi\left(\theta_s - \theta_f\right) = 0, \tag{5}$$

where the following non-dimensional variables are used:

$$X,Y = \frac{x,y}{D}, \quad U = \frac{uD}{\alpha_f}, \quad V = \frac{vD}{\alpha_f}, \quad \theta = \frac{(T-T_c)}{(T_h-T_c)}, \quad P_f = \frac{p_f D^2}{\rho_f \alpha_f^2}. \tag{6}$$

Here, U and V are the dimensionless velocity components along the X- and Y-axes, θ is the dimensionless temperature field, P_f is the dimensionless fluid pressure field and ε is the porosity. Subscripts f and s denote the fluid and solid phases, respectively. The dimensionless groups, i.e., Rayleigh, Darcy, Prandtl, Biot numbers and solid/fluid thermal conductivity ratio, appearing in Eqs. (1)–(5), constitute the key parameters of the problem as follows:

$$Ra = \frac{g\beta D^3(T_h-T_c)}{\alpha_f \nu_f}, \quad Da = \frac{K}{D^2}, \quad Pr = \frac{\nu_f}{\alpha_f}, \quad Bi = \frac{D^2 h_{sf} a_{sf}}{k_s}, \quad k_r = \frac{k_s}{k_f}, \tag{7}$$

where K and C_F are the permeability and the inertia coefficients, respectively, of the porous medium. They are based on Ergun's empirical expression [6], which may be used for packed beds that may be closely modelled as spherical beads of diameter d. The coefficients are given by:

$$K = \frac{\varepsilon^3 d^2}{150(1-\varepsilon)^2}, \quad C_F = \frac{1.75}{\sqrt{150\varepsilon^3}}, \tag{8}$$

where, a_{sf} and h_{sf} are the specific surface area of the particles and the fluid-to-particle heat transfer coefficient, respectively, in the packed bed. They can be modelled using the correlations proposed by Dullien [4] for a_{sf}, and by Wakao et al. [23] for h_{sf} as follows:

$$a_{sf} = \frac{6(1-\varepsilon)}{d}, \tag{9}$$

$$h_{sf} = \frac{k_f}{d}\left(2 + Pr^{1/3}Re_p^{0.6}\right), \tag{10}$$

where, Re_p is the *particle Reynolds number*

$$Re_p = \frac{\rho_f|u|d}{\mu_f}. \tag{11}$$

In the present study, the dispersion phenomenon, in both longitudinal and lateral directions, is treated as an additional diffusive term added to the fluid stagnant component. The stagnant component is expressed in terms of the phase porosities and their thermal conductivities. The empirical correlation developed by Wakao and Kaguei [22] is employed in this study to model the fluid effective conductivities:

$$\frac{k_{f.eff,(x)}}{k_f} = \varepsilon k_f + 0.5\ Pr\ Re_p, \tag{12}$$

$$\frac{k_{f.eff,(y)}}{k_f} = \varepsilon k_f + 0.1\ Pr\ Re_p, \tag{13}$$

$$\frac{k_{s.eff}}{k_s} = (1-\varepsilon). \tag{14}$$

The fluid motion is displayed using the stream function Ψ obtained from the velocity components U and V. The relationships between the stream function and the velocity components are $U = \partial\Psi/\partial Y$ and

$V = -\partial\Psi/\partial X$. We assume $U = V = 0$ on all boundaries. The boundary conditions for the non-dimensional temperatures are:

$$
\begin{aligned}
\theta_f = \theta_s = 0 & \quad \text{at } (X = 0 \text{ and } L, 0 < Y < H), \\
\theta_f = \theta_s = 0 & \quad \text{at } (Y = H, 0 < X < L), \\
\frac{\partial\theta_f}{\partial Y} = \frac{\partial\theta_s}{\partial Y} = 0 & \quad \text{at } (Y = 0, 0 < X < L), \\
\theta_f = \theta_s = 1 & \quad \text{at the cylinder boundary } (0 < \varphi^o < 360).
\end{aligned}
\tag{15}
$$

The physical quantity of interest in this problem is the heat transfer rate. The heat transfer rate distribution is obtained by applying Fourier's law at the heated cylinder wall, i.e.,

$$
q_f = -\frac{k_{f.eff}}{k_f}\frac{\partial T_f}{\partial n}, \quad q_s = -\frac{k_{s.eff}}{k_s}\frac{\partial T_s}{\partial n}.
\tag{16}
$$

Eq. (16) can become in terms of the dimensionless variables,

$$
\begin{aligned}
Nu_f = \frac{q_f D}{(T_h - T_c)} = \frac{1}{S}\int_0^S \frac{k_{f.eff}}{k_f}\frac{\partial\theta_f}{\partial n}\,ds, \\
Nu_s = \frac{q_s D}{(T_h - T_c)} = \frac{1}{S}\int_0^S \frac{k_{s.eff}}{k_s}\frac{\partial\theta_s}{\partial n}\,ds,
\end{aligned}
\tag{17}
$$

where n and s denote to the normal and tangential directions at the cylinder surface, respectively, S is the circumference of the cylinder, and Nu_f and Nu_s are the fluid and solid Nusselt numbers, respectively. Consequently, the total Nusselt number Nu_t is defined as the summation of Nu_f and Nu_s:

$$
Nu_t = Nu_f + Nu_s.
\tag{18}
$$

4. Numerical method

The system of Eqs. (1)–(5) along with the boundary conditions, i.e., Eq. (15), have been solved numerically using the nodal-based spectral-element method. This method is a high-order Galerkin finite-element approach, and is well-documented by, for example, Fletcher [8], Fletcher [9] and Karniadakis and Sherwin [13]. In this method, the computational domain is usually subdivided coarsely into a series of discrete macro-elements, as shown in Fig. 2. Nodes internal to each macro-element are distributed according to the Gauss–Legendre–Lobatto quadrature points; the accuracy of the simulation can be improved by incrementing the polynomial order p, where $N = p + 1$ is the number of interior node points in each direction within each macro-element. Therefore,
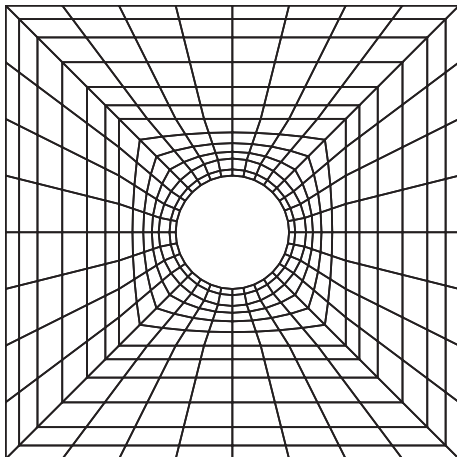

Fig. 2. Computational macro-element mesh used. Note that each element is further subdivided internally.

Table 1
Grid resolution study of the computational domain, at two values of Rayleigh number, $Ra = 10^4$ and 10^7. This is done by varying the interpolation polynomial order p within the range 2–7, while keeping the macro-element layout the same.

$p(N \times N)$	$Ra = 10^4$		$Ra = 10^7$	
	Nu_f	Nu_s	Nu_f	Nu_s
2 (3 × 3)	1.2597	0.63011	3.5617	0.75082
3 (4 × 4)	1.2554	0.62794	3.5594	0.74977
4 (5 × 5)	1.2515	0.62601	3.5551	0.74831
5 (6 × 6)	1.2490	0.62475	3.5514	0.74724
6 (7 × 7)	1.2473	0.62388	3.5480	0.74640
7 (8 × 8)	1.2460	0.62365	3.5466	0.74624

numerical runs have been conducted to ensure that the numerical results obtained are independent of the spatial grid resolution. The results shown in Table 1 indicate that Nu_f and Nu_s are converged by $p = 6$ with a relative error of less than 0.4%. Thereby, all the results shown in this paper have been run with polynomial order $p = 6$.

In order to test the accuracy of the computational code, that has been also used and thoroughly verified in our works Al-Sumaily et al. [1] and Al-Sumaily et al. [2], previously published for the case of forced convection heat transfer from a circular cylinder embedded in a porous medium, we have compared the code's predictions with the results of Pop et al. [18], Yih [24] and Kumari and Jayanthi [14], for the case of natural convection around a cylinder placed in a porous medium in classical thermal equilibrium. The thermally equilibrium model is recovered in the present formulation by setting $Bi = 0$ and assuming that the energy equation of the fluid phase represents the energy balance of both fluid and solid phases. The results, which are presented in Table 2, are found to be in good agreement.

5. Results and discussion

Steady-state free convection heat transfer in the system under consideration is dependent on several independent parameters. In the present study, the effects of two pertinent independent parameters have been investigated: Rayleigh number $Ra \in [10^3, 5 \times 10^7]$ and solid-to-fluid thermal conductivity ratio $k_r \in [0.01, 10000]$ which covers a wide range of metallic and non-metallic porous materials. Air is chosen as the working fluid with $k_f = 0.025$ W/m · K and $Pr = 0.71$. The physical properties of the porous medium used have been selected to be constant in this study as follows: cylinder-to-particle diameter ratio

Table 2
Comparison of the heat transfer parameter ($Nu/\sqrt{Ra}$) at the cylinder wall with values from references for the thermal equilibrium model.

| φ (rad)	Present results	Pop et al. [18]	Yih [24]	Kumari and Jayanthi [14]
0.0	0.62766	0.6272	0.6276	0.6274
0.2	0.62454	0.6295	0.6245	0.6245
0.4	0.61518	0.6202	0.6151	0.6151
0.6	0.59964	0.6048	0.5996	0.5996
0.8	0.57817	0.5834	0.5781	0.5781
1.0	0.55083	0.5562	0.5508	0.5509
1.2	0.51807	0.5236	0.5180	0.5181
1.4	0.48009	0.4859	0.4800	0.4801
1.6	0.43728	0.4433	0.4371	0.4374
1.8	0.38999	0.3964	0.3899	0.3903
2.0	0.33882	0.3456	0.3387	0.3393
2.2	0.28445	0.2913	0.2843	0.2849
2.4	0.22722	0.2339	0.2271	0.2276
2.6	0.16778	0.1741	0.1677	0.1681
2.8	0.10660	0.1119	0.1066	0.1068
3.0	0.04461	0.0477	0.0446	0.0445
π	0.00011	0.0005	0.0001	0.0001
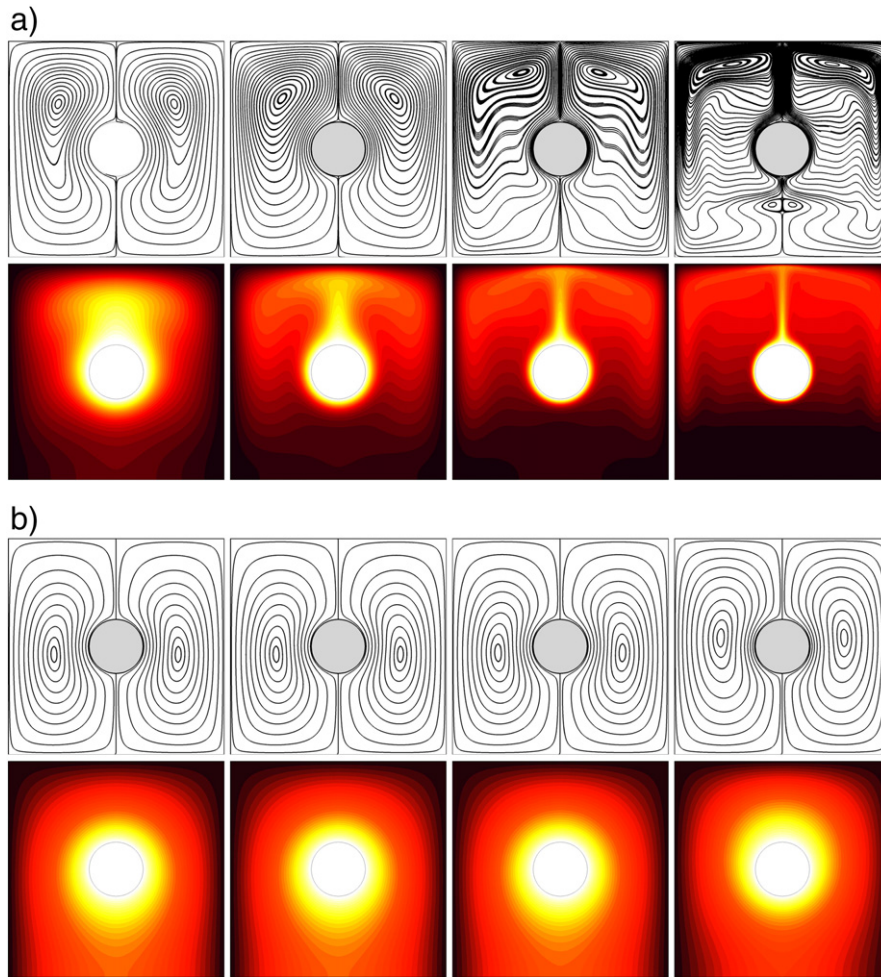
Fig. 3. Flow (streamlines) and thermal fields in the empty cavity (top), and the packed bed (bottom), for a range of Ra, and with $k_r = 1.0$ for the porous bed.

$D/d = 20$, porosity $\varepsilon = 0.5$, and as a consequence, the Darcy number is $Da = 8.333 \times 10^{-6}$.

Figs. 3 and 4 show the effect of Ra on the flow, and the thermal fields and the heat transfer rates released from the cylinder, in terms of streamlines, isotherms and Nusselt numbers, respectively, in an enclosure with and without the presence of the porous medium. This comparison between both empty (non-filled) and porous medium filled enclosures has been performed for a limited range of Rayleigh number ($Ra = 10^3 - 10^6$). The reason for choosing this range is that it was found to be not possible to obtain numerical convergence in the empty cavity for $Ra > 10^6$ due to the high instability in the flow, caused by high-intensity recirculations above the cylinder. In the porous enclosure, the results of these two figures have been obtained at $k_r = 1.0$. For various selected values of Ra between 10^3 and 10^6, the flow patterns in Fig. 3 are characterised by two symmetrical rolls with anti-clockwise ($+$) and clockwise ($-$) rotation inside the enclosures. These cells intersect along the vertical centreline of the enclosure. The hot fluid rises from the cylinder surface to the central top region as a result of buoyancy, but is blocked at the cold top wall. It then descends along the cold side walls and turns horizontally to the central bottom region after hitting the bottom adiabatic wall. Thus, a pair of counter-rotating rolls is formed in the flow domain in both cavities. However, it is obvious that the intensity of the flow inside the empty cavity is much stronger than that in the packed bed for all Ra. This can be explained by the different thermal responses in the enclosures as Ra increases. For example, in the empty enclosure, it can be seen in Fig. 3a that at higher Ra, the intensity of convection increases significantly, where the core of the

circulating rolls moves up considerably, i.e., at $Ra = 10^6$, it is strongly compressed and deformed by the top wall, which is associated with stronger buoyant forces that intensify the circulating cells. This makes
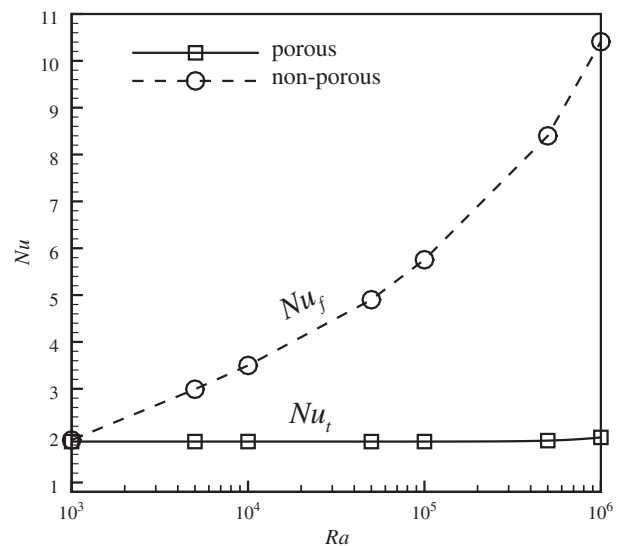

Fig. 4. Variation of heat transfer rates from a heated cylinder with Ra, for the cylinder mounted in an enclosure with and without the presence of porous media.
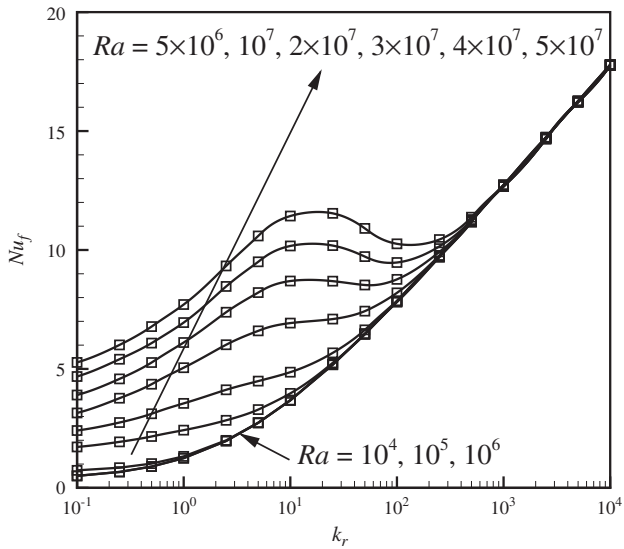
Fig. 5. Variation of fluid Nusselt number Nu_f from the cylinder against k_r in the porous cavity at different Ra.

the isotherm patterns change significantly, indicating that convection is the dominating heat transfer mechanism in the enclosure. On the other hand, in the packed bed, as can be expected, the heat transfer from the hot cylinder is essentially dissipated via a conduction-dominated mechanism due to the presence of the solid spheres filling the cavity, as indicated by the isotherm pattern shown in Fig. 3b. Therefore, in the flow images of Fig. 3b, the locations of the cores of the rolls are almost identical.

Fig. 4 shows that the heat transfer rate increases significantly with increasing Ra in the empty enclosure due to the high convection that causes intensified thermal boundary layers around the cylinder, as demonstrated in Fig. 3a. This increases the temperature gradient on the cylinder surface, and then increases the average Nusselt number Nu_f as described through Eq. (17). However, in the porous enclosure, it is shown that the total heat transfer rate Nu_t, throughout both fluid and solid phases, remains approximately constant over the Rayleigh number range of the study. Within this range, the convection from the heat source is low, and most of the thermal energy transfers throughout the two phases of the porous medium by conduction, as previously mentioned. Also, there is an inter-phase heat convection from the solid to the fluid phase, which increases the fluid thermal boundary layer in the vicinity of the hot cylinder. These are the main influences on the fluid temperature around the cylinder, as seen in Fig. 3b. Moreover, for $kr_r = 1.0$, it is interesting to note that introducing the porous medium into the empty cavity significantly reduces the heat transfer rates for $Ra > 10^3$. As can be seen, this reduction in Nu increases as Ra increases, and its maximum value is obtained at higher $Ra = 10^6$ (up to five times compared with the empty enclosure). It indicates that this kind of porous media can be used as an insulator for heat transfer in engineering thermal applications. The effect of using different porous
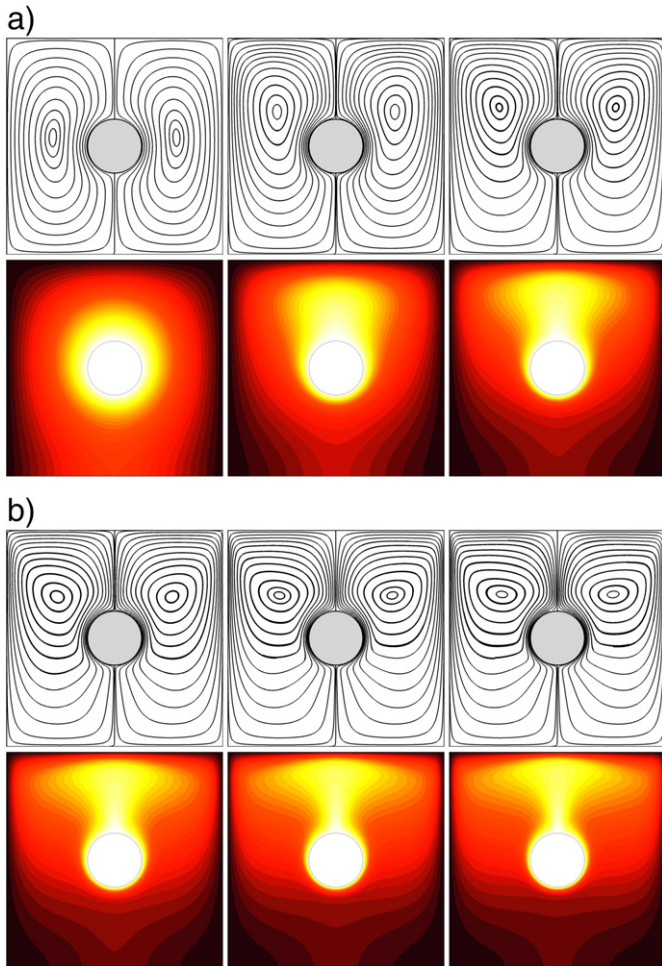

Fig. 6. Fluid thermal response and stream lines in the porous cavity at higher Rayleigh numbers $10^6 \leq Ra \leq 4 \times 10^7$, and at $k_r = 1.0$.
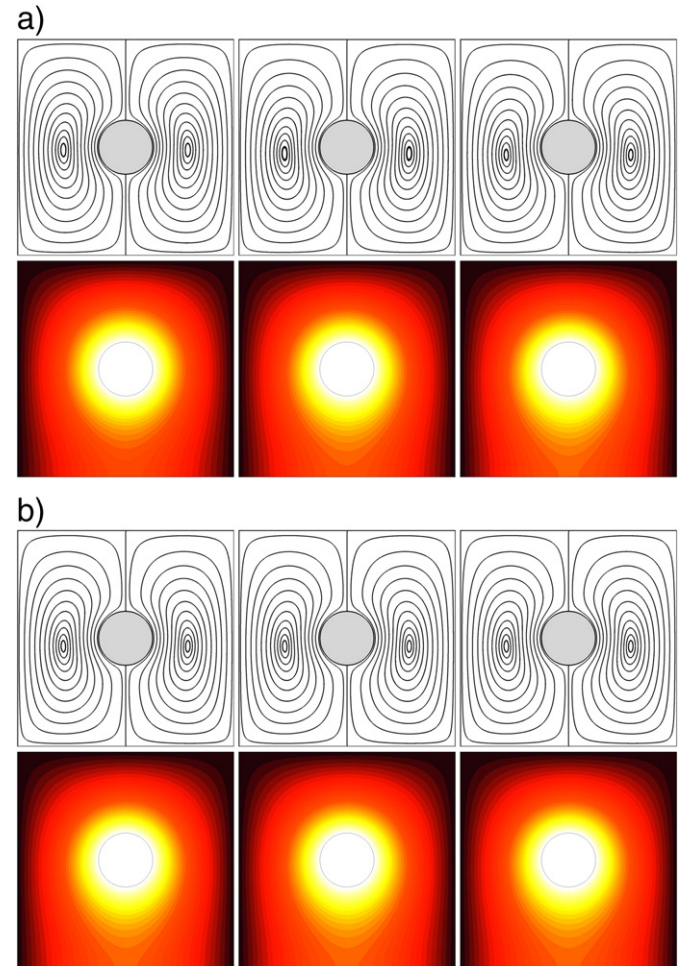

Fig. 7. Fluid temperature distribution and stream lines in the porous cavity for the entire range of $k_r = 0.1 - 10000$, and at $Ra = 10^5$.

materials on Nu, and at higher Rayleigh numbers has been also investigated, and the results are shown in the next figures.

The variations of fluid Nusselt number Nu_f with solid-to-fluid thermal conductivity ratio k_r (representative of different porous materials) are shown in Fig. 5. The curves correspond to different Rayleigh numbers in the range $Ra = 10^4 - 5 \times 10^7$. In this figure, it is observed that there is generally an increase in Nu_f for an increase in k_r for all values of Ra. The figure also shows that, for fixed kr_r, a greater increase in heat transfer rates can be obtained for the higher range of Ra, but with a local maximum occurring for values $k_r = 10 - 25$. However, at least for this range of Rayleigh number, the effect of Ra on Nu_f disappears for $k_r \geq 250$, and for smaller values of Ra ($10^3 - 10^6$) there is a little effect for the entire range of k_r. An interesting observation from Fig. 5 is that at $Ra = 10^6$, Nu_f increases from 2 to 18 as k_r increases from 1 to 10,000. This increased value of Nu_f is seen to be considerably higher than that for the case without a porous medium, as depicted in Fig. 4. This means that the porous particles with higher thermal conductivity serve as effective enhancers for free convection heat transfer.

For $kr_r = 1.0$, the influence of using higher Rayleigh numbers $10^6 \leq Ra \leq 4 \times 10^7$ on the fluid thermal and flow fields in the porous enclosure, is shown in Fig. 6. It can be seen that a laminar thermal plume moves away from the cylinder towards the top ceiling for $Ra > 10^6$. The strength of the plume increases as Ra increases, and for $Ra > 10^7$ it spreads relatively thinly along the cavity ceiling. This affects the location of the flow recirculations, with their centres moving towards the top of the cavity as the Rayleigh number increases. The shapes of these vortical flow patterns also change from vertically to horizontally aligned due to the increasing dominance of buoyancy on the induced flows.

Under the assumption of *Local Thermal Equilibrium*, it is well recognised in the literature that heat transfer can be increased by using porous media with higher thermal conductivity. However, it is also documented that these kinds of high conductivity materials in a *Local Thermal non-Equilibrium* porous system produce a highly uniform thermal field in the fluid phase around the heat source, see e.g. Al-Sumaily et al. [1]. This is because of the large contribution to heat transfer from the solid to the fluid phase through convection, as h_{sf} is taken into account in this system. The result of this can be seen in Fig. 7. In this figure, which is produced for $Ra = 10^5$, it is seen that as k_r increases, a uniform fluid thermal boundary layer (*FTBL*) is generated around the hot cylinder. Indeed, at high values of k_r, the thickness of this *FTBL* increases rather than decreases. This means that a decrease in Nu_f should be registered as k_r increases, due to the decrease in the fluid temperature gradient, $(\partial \theta_f/\partial n)$ in Eq. (17), as its *FTBL* increases in thickness. These ideas are clarified for high Rayleigh number cases, as shown in Fig. 8 at $Ra = 2 \times 10^7$. For low k_r, the convective contribution from the solid phase ceases (becomes insulated), and the increased convection in the fluid phase, from stronger buoyancy forces generated at high Ra, dominates. However, as k_r is increased to high values, the heat transfer from the solid to the fluid phase begins to increase (good conductor), causing a warm fluid domain that reduces the convection effect.

Fig. 9 better clarifies the effect of k_r on the fluid temperature gradient $(\partial \theta_f/\partial n)$ for the hot cylinder surface at different Ra. As can be seen, and
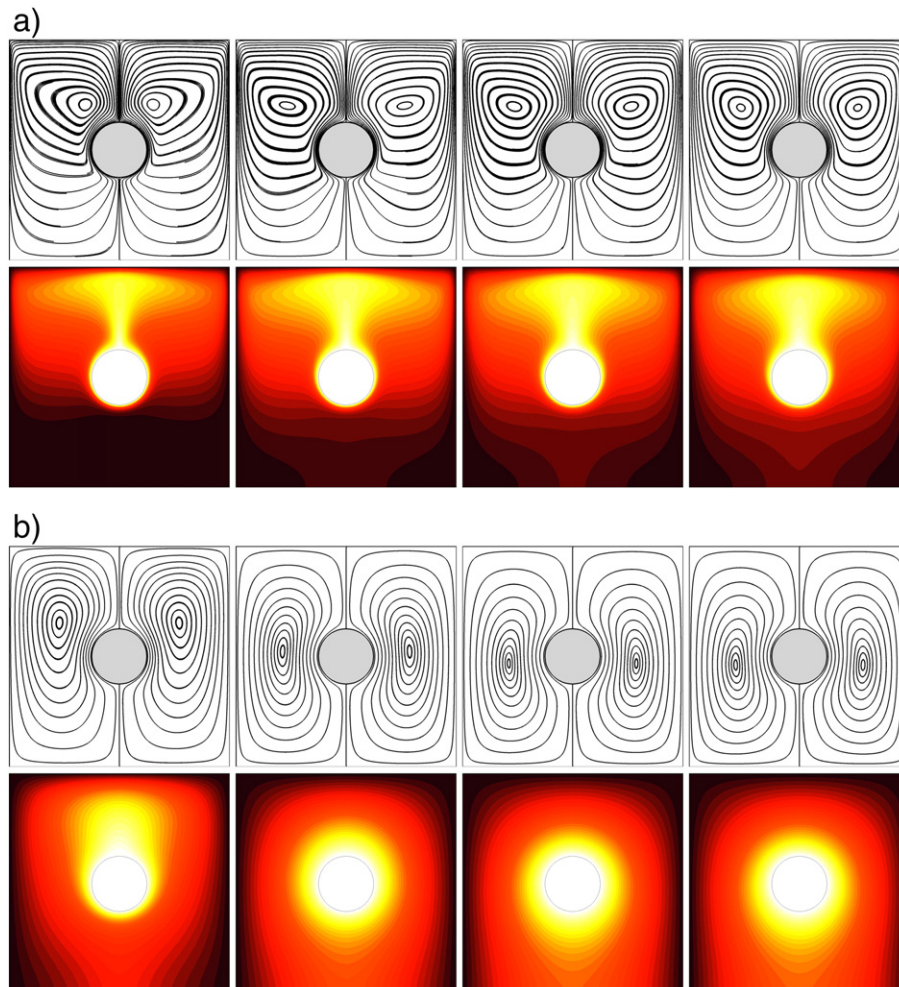

Fig. 8. Fluid temperature distribution and stream lines in the porous cavity for the entire range of $kr = 0.1$–10,000, and at $Ra = 2 \times 10^7$.
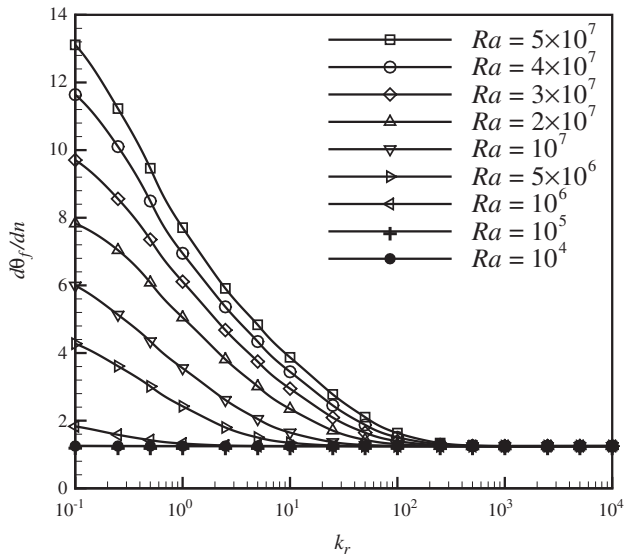
Fig. 9. Variation of fluid temperature gradient around the cylinder surface with k_r at different Ra.

as mentioned above, this effect becomes significant at high Ra and is diminished at low Ra, i.e., ($\leq 10^5$). Then, the question can be raised: What is the main reason for the substantial increase in Nu_f with k_r if it is not coming from the decreasing $\partial\theta_f/\partial n$? The answer comes from considering the contribution of the fluid effective thermal conductivity $k_{f.\ eff}$ on the calculation of Nu_f in Eq. (17), which appears to have a stronger influence than that directly through $\partial\theta_f/\partial n$.

Fig. 10 shows the variations of solid Nusselt number Nu_s with k_r, for different values of Ra. It reveals that low values of Nu_s are produced when k_r is large. This is as expected since it means that there is a high transient heat conduction within the solid phase when k_r is increased, which increases the thickness of the solid thermal boundary layer ($STBL$) at the steady-state condition, and then decreases Nu_s. This also could explain the better transient convective heat transfer between the two phases (from the solid to the fluid for large k_r), which also increases the thickness of the $FTBL$, and then decreases $\partial\theta_f/\partial n$ as shown in Fig. 9. However, small values of k_r correspond to poor transfer of
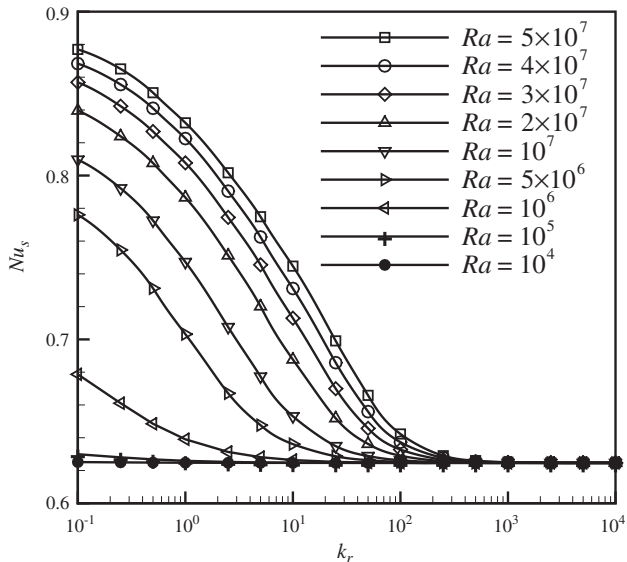
inter-phase heat from the solid phase, which enables its thermal field to be effectively independent of the fluid thermal field.

6. Conclusion

The present numerical study investigates the effect of packing an empty enclosure with spherical particles on buoyancy-induced flow, and temperature fields and heat transfer, from a heated cylinder mounted inside it, for varying Rayleigh number and thermal conductivity ratio. Importantly, local thermal equilibrium between the solid and fluid phases is not assumed. The following major conclusions are drawn as: The existence of the porous medium suppresses the strong convection and the associated high intensity vortices behind the cylinder, due to the high frictional and inertial resistances offered by the matrix of the porous particles. In the empty enclosure, within the chosen range of Ra, i.e., ($10^3 - 10^6$), it is shown that the effect of Ra on the thicknesses of the fluid thermal and hydrodynamic boundary layers is very significant, and any increase in Ra produces a considerable increase in Nu_f, due to the reduction in these thicknesses. However, in the porous enclosure with $kr_r = 1$, the effect is found to be almost negligible for $Ra \leq 10^6$; but for $Ra > 10^6$, its influence on these two layers, and consequently on heat transfer, becomes considerable. In addition, it is found that at any Ra, the effect of increasing k_r is to increase the thicknesses of the $FTBL$ and $STBL$, and thus decrease their temperature gradients at the hot surface, which means a decrease in both Nu_f and Nu_s. However, the results show that using high conductivity porous materials, i.e., $k_r > 100$, causes a better enhancement of heat transfer in the fluid phase Nu_f, (*enhancer for heat transfer*), and vice versa (*insulator for heat transfer*) for low k_r. Indeed, the increase or decrease in Nu_f as k_r increases or decreases, respectively, is not controlled by the $FTBL$, but is due to the fluid effective thermal conductivity entering the equation defining Nu_f.

References

[1] G.F. Al-Sumaily, A. Nakayama, J. Sheridan, M.C. Thompson, The effect of porous media particle size on forced convection from a circular cylinder without assuming local thermal equilibrium between phases, Int. J. Heat Mass Transf. 55 (13–14) (2012) 3366–3378.

[2] G.F. Al-Sumaily, J. Sheridan, M.C. Thompson, Analysis of forced convection heat transfer from a circular cylinder embedded in a porous medium, Int. J. Therm. Sci. 51 (2012) 121–131.

[3] P. Cheng, Natural convection in a porous medium: external flows, in: S. Kakac, W. Aung, R. Viskanta (Eds.), Natural Convection: Fundamentals and Applications, Martinus Nijhoff, The Hague, The Netherlands, 1985, pp. 453–475.

[4] F.A. Dullien, Media Fluid Transport and Pore Structure, Academic Press, New York, 1979.

[5] E.R.G. Eckert, R.M. Drake, Analysis of Heat and Mass Transfer, McGraw-Hill, New York, 1972.

[6] S. Ergun, Fluid flow through packed columns, Chem. Eng. Prog. 48 (2) (1952) 89–94.

[7] R.M. Fand, T.E. Steinberger, P. Cheng, Natural convection heat transfer from a horizontal cylinder embedded in a porous medium, Int. J. Heat Mass Transf. 29 (1) (1986) 119–133.

[8] C.A.J. Fletcher, Computational Galerkin Methods, Springer-Verlag, New York, 1984.

[9] C.A.J. Fletcher, Computational Techniques for Fluid Dynamics, vol. 1, Springer-Verlag, New York, 1991.

[10] K. Himasekhar, H.H. Bau, Thermal convection around a heated source embedded in a box containing a saturated porous medium, J. Heat Transf. 110 (3) (1988) 649–654.

[11] S.W. Hsiao, P. Cheng, C.K. Chen, Non-uniform porosity and thermal dispersion effects on natural convection about a heated horizontal cylinder in an enclosed porous medium, Int. J. Heat Mass Transf. 35 (12) (1992) 3407–3418.

[12] D.B. Ingham, I. Pop, Natural convection about a heated horizontal cylinder in a porous medium, J. Fluid Mech. 184 (1987) 157–181.

[13] G.E. Karniadakis, S.J. Sherwin, Spectral/hp Methods for Computational Fluid Dynamics, Oxford University Press, Oxford, 2005.

[14] M. Kumari, S. Jayanthi, Non-Darcy non-Newtonian free convection flow over a horizontal cylinder in a saturated porous medium, Int. Commun. Heat Mass Transfer 31 (8) (2004) 1219–1226.

[15] M. Kumari, G. Nath, Unsteady natural convection flow over a heated cylinder buried in a fluid saturated porous medium, J. Porous Media 12 (12) (2009) 1225–1235.

[16] J.H. Merkin, Free convection boundary layers on axi-symmetric and two-dimensional bodies of arbitrary shape in a saturated porous medium, Int. J. Heat Mass Transf. 22 (10) (1979) 1461–1462.

Fig. 10. Variation of solid Nusselt number Nu_s from the cylinder against k_r in the porous enclosure, at different Ra.

[17] P.H. Oosthuizen, D. Naylor, Natural convective heat transfer from a cylinder in an enclosure partly filled with a porous medium, Int. J. Numer. Methods Heat Fluid Flow 6 (6) (1996) 51–63.

[18] I. Pop, M. Kumari, G. Nath, Free convection about cylinders of elliptic cross section embedded in a porous medium, Int. J. Eng. Sci. 30 (1) (1992) 35–45.

[19] M.A. Saada, S. Chikh, A. Campo, Natural convection around a horizontal solid cylinder wrapped with a layer of fibrous or porous material, Int. J. Heat Fluid Flow 28 (3) (2007) 483–495.

[20] N.H. Saeid, Analysis of free convection about a horizontal cylinder in a porous media using a thermal non-equilibrium model, Int. Commun. Heat Mass Transfer 33 (2) (2006) 158–165.

[21] R. Thiyagarajan, M.M. Yovanovich, Thermal resistance of a buried cylinder with constant flux boundary condition, J. Heat Transf. 96 (1974) 249–250.

[22] N. Wakao, S. Kaguei, Heat and Mass Transfer in Packed Beds, Gordon and Breach, New York, 1982.

[23] N. Wakao, S. Kaguei, T. Funazkri, Effect of fluid dispersion coefficients on particle-to-fluid heat transfer coefficients in packed beds-correlation of Nusselt numbers, Chem. Eng. Sci. 34 (3) (1979) 325–336.

[24] K. Yih, Coupled heat and mass transfer by natural convection adjacent to a permeable horizontal cylinder in a saturated porous medium, Int. Commun. Heat Mass Transfer 26 (3) (1999) 431–440.